Biochemistry

The Mechanism of Acetyl Transfer Catalyzed by *Mycobacterium tuberculosis* GlmU

Peter D. Craggs,[†,§] Stephane Mouilleron,[‡] Martin Rejzek,[∥] Cesira de Chiara,[†] Robert J. Young,[§] Robert A. Field,[∥] Argyrides Argyrou,*[,§,⊥] and Luiz Pedro S. de Carvalho*[,†]

[†]Mycobacterial Metabolism and Antibiotic Research Laboratory and [‡]Structural Biology Scientific Technology Platform, The Francis Crick Institute, London, U.K.

[§]Platform Technology and Science, GlaxoSmithKline, Stevenage, U.K.

[∥]John Innes Centre, Norwich, U.K.

S *Supporting Information*
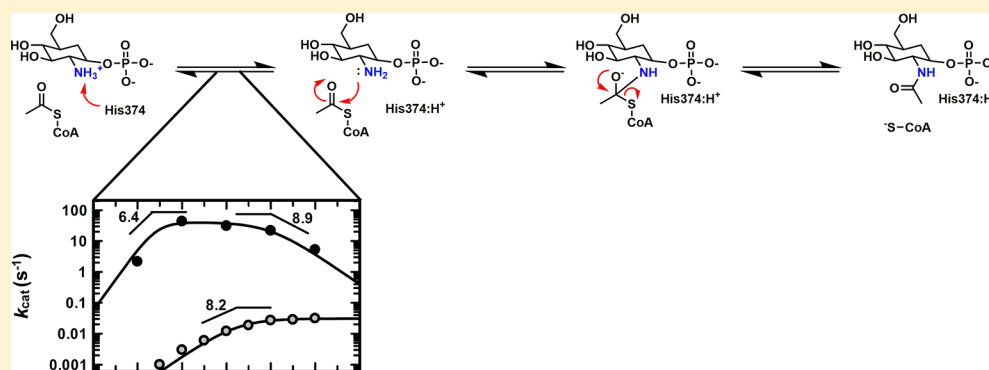
ABSTRACT: The biosynthetic pathway of peptidoglycan is essential for *Mycobacterium tuberculosis*. We report here the acetyltransferase substrate specificity and catalytic mechanism of the bifunctional *N*-acetyltransferase/uridylyltransferase from *M. tuberculosis* (GlmU). This enzyme is responsible for the final two steps of the synthesis of UDP-*N*-acetylglucosamine, which is an essential precursor of peptidoglycan, from glucosamine 1-phosphate, acetyl-coenzyme A, and uridine 5′-triphosphate. GlmU utilizes ternary complex formation to transfer an acetyl from acetyl-coenzyme A to glucosamine 1-phosphate to form *N*-acetylglucosamine 1-phosphate. Steady-state kinetic studies and equilibrium binding experiments indicate that GlmU follows a steady-state ordered kinetic mechanism, with acetyl-coenzyme A binding first, which triggers a conformational change in GlmU, followed by glucosamine 1-phosphate binding. Coenzyme A is the last product to dissociate. Chemistry is partially rate-limiting as indicated by pH−rate studies and solvent kinetic isotope effects. A novel crystal structure of a mimic of the Michaelis complex, with glucose 1-phosphate and acetyl-coenzyme A, helps us to propose the residues involved in deprotonation of glucosamine 1-phosphate and the loop movement that likely generates the active site required for glucosamine 1-phosphate to bind. Together, these results pave the way for the rational discovery of improved inhibitors against *M. tuberculosis* GlmU, some of which might become candidates for antibiotic discovery programs.

Human tuberculosis (TB), caused by *Mycobacterium tuberculosis*, is one of the most persistent and devastating infectious human diseases of all time and leads to an estimated 1.8 million deaths per year, mainly in the developing world. The World Health Organisation recently reported that in 2016 TB was the ninth leading cause of death worldwide, with an estimated 10.4 million new cases of TB and 490000 incidences of multidrug-resistant TB (MDR-TB).[1] The incidence of TB-related deaths, the emergence and dissemination of drug-resistant TB, and complications due to HIV co-infection highlight the dire need to identify novel chemotherapeutic agents to complement or replace the current therapies, reduce the 6 month treatment time, and minimize the adverse side effects of the existing regimens.[2]

A defining characteristic of *M. tuberculosis* is its unique and complex cell envelope structure.[3] The cell wall core consists of three primary components: an inner layer of the cross-linked polymer of peptidoglycan, which is covalently attached to a middle section of highly branched arabinogalactan polysaccharide that is in turn esterified with an outer coating of long chain mycolic acids.[4] The cell wall is covered in two additional layers: an outer membrane, comprised of noncovalently linked glycophospholipids and inert waxes, and a loosely attached
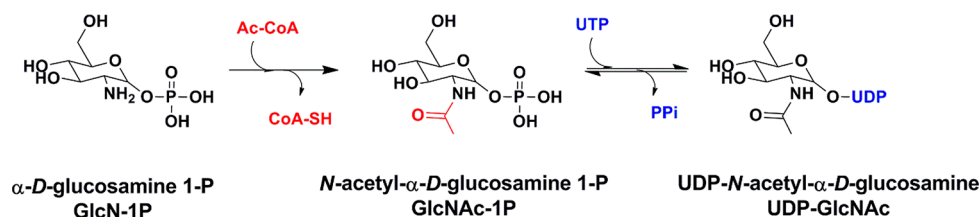
Scheme 1. Overall Reactions Catalyzed by GlmU

capsule, consisting of polysaccharides, proteins, and a minor amount of lipids.[5] The biosynthesis of this complex cell envelope is comprised of a number of essential individual pathways, some of which have already been exploited as targets for chemotherapeutics, such as isoniazid (mycolic acid synthesis) and D-cycloserine (peptidoglycan). In spite of that, many more of these pathways remain underexplored and are the potential source of new, attractive, *M. tuberculosis* drug targets.[6−8]

UDP-*N*-acetylglucosamine (UDP-GlcNAc) is an essential precursor of cell wall peptidoglycan (PG) in mycobacteria, and its formation in the cytoplasm from D-fructose 6-phosphate in a four-stage, three-enzyme biosynthetic pathway is considered the first step of PG biosynthesis.[9] The three enzymes involved in the UDP-GlcNAc biosynthetic pathway are glucosamine-6-phosphate synthase (GlmS), phosphoglucosamine mutase (GlmM), and the bifunctional *N*-acetyl-glucosamine-1-phosphate acetyltransferase uridylyltransferase (GlmU). GlmS is a glutamine-dependent amidotransferase that catalyzes the formation of D-glucosamine 6-phosphate from L-glutamine and D-fructose 6-phosphate.[10] GlmM catalyzes the interconversion of D-glucosamine 6-phosphate to D-glucosamine 1-phosphate.[11] GlmU is a bifunctional enzyme that catalyzes the N-acetylation of glucosamine 1-phosphate (GlcN1-P), and the uridylylation of *N*-acetyl-glucosamine 1-phosphate (GlcNAc-1P) to form UDP-GlcNAc (Scheme 1).

The synthesis pathway of UDP-GlcNAc and the enzymes involved in this process were first identified in *Escherichia coli* in 1993, and in subsequent studies in 1994, GlmU was purified for the first time and the kinetic parameters of the bifunctional activities were characterized.[12,13] The structure of *E. coli* GlmU was determined in 2001, revealing a trimeric arrangement and identifying a two-domain architecture.[14] Subsequently, the structures of GlmU orthologues from a number of bacteria, including *Streptococcus pneumoniae* [Protein Data Bank (PDB) entry 1G95], *Haemophilus influenzae* (PDB entry 2V0H), and *M. tuberculosis* (PDB entry 3D98), have been determined.[15−17] These structures show a high degree of similarity with the *E. coli* orthologue and reveal that the monomer of GlmU is folded into two distinct domains. The C-terminal domain (residues 263−478) is a left-handed *β*-helix (L*β*H), which is similar to a number of acetyltransferase enzymes, such as serine acetyltransferase, galactoside acetyltransferase, maltose acetyltransferase, LpxA, and LpxD, which make up the L*β*H superfamily.[18−23] Proteins belonging to the L*β*H superfamily have a structure comprising a parallel *β*-helix with repeating isoleucine-rich hexapeptide motifs and left-handed connections. The C-terminal acetyltransferase domain catalyzes the synthesis of GlcNAc1-P from GlcN1-P and acetyl-Coenzyme A (Ac-CoA), while the N-terminal domain (residues 2−262) contains a dinucleotide binding Rossmann fold, which is a typical fold found in uridylyltransferases. The N-terminal domain catalyzes

the formation of *N*-acetyl-glucosamine 1-phosphate (UDP-GlcNAc) from GlcNAc1-P and UTP.

The *M. tuberculosis glmU* gene encodes a 51.6 kDa protein, which is enzymatically active as a trimer in solution. Protomers cannot be active as the C-terminal acetyltransferase site contains contributions from all three subunits. The truncation of the C-terminal region leads to ablation of nearly all activity from both domains, indicating that the multimeric structure is required for optimal activity.[24] The two domains are joined by a long *α*-helical arm of 22 residues, suggesting that GlmU evolved by fusion of uridylyltransferase- and acetyltransferase-encoding genes. In eukaryotes, the biosynthesis of UDP-GlcNAc occurs by a different route [via *N*-acetyl-D-glucosamine 6-phosphate (GlcNAc-6P)] in which GlcN-6P acetyltransferase and GlcNAc-1P uridylyltransferase activities are carried by two distinct monofunctional enzymes.[25−27] There are no reports that demonstrate a selective advantage conferred to bacteria by the bifunctional arrangement of GlmU over separate enzymes, and there is little evidence for cooperativity or cross-talk between the two catalytic domains.[28]

Transposon site hybridization mutagenesis studies by Sassetti et al. in 2003 identified GlmU as one of seven essential genes of the 10 genes involved in peptidoglycan biosynthesis in *M. tuberculosis*.[29] These data were further supported by results from studies with *Mycobacterium smegmatis* that demonstrated that GlmU deletions in this fast-grower mycobacteria were unable to grow.[30] Recently, homologous recombination studies of *glmU* in *M. tuberculosis* demonstrated that the acetyltransferase and uridylyltransferase activities of GlmU are independently essential for bacterial survival *in vitro*, as well as ascertaining that GlmU is also essential for mycobacterial survival in THP-1 cells as well as in guinea pigs.[31] These results strongly support the essentiality of GlmU and provide genetic validation of this bifunctional enzyme as a high-value target for the development of novel antitubercular agents.

In contrast to its now validated role in *M. tuberculosis*, little is known about the kinetic and chemical mechanisms of GlmU. The extensive structural studies of the different orthologues of GlmU, including the *M. tuberculosis* variant, have identified a number of substrate−enzyme complexes, which serve to identify residues involved in substrate binding and potentially in catalysis.[32] However, the kinetic and chemical mechanism of *M. tuberculosis* GlmU activities remains undefined.

In this study, we have explored the GlmU-catalyzed acetyl transfer reaction through a combination of steady-state kinetics, pH−rate studies, equilibrium binding techniques, solvent kinetic isotope effects (SKIEs), and X-ray crystallography.

■ MATERIALS AND METHODS

Materials. All details can be found in the Supporting Information.

Synthesis of UDP-*α*-D-glucosamine (UDP-GlcN). The chemical synthesis of UDP-GlcN was performed using a

modification of a method previously described by Morais et al.,[33] the details of which can be found in the Supporting Information.

Measurement of Acetyltransferase Enzymatic Activity. Initial velocities for the forward acetyltransferase reaction of GlmU were performed at 30 °C using 4,4′-dithiodipyridine (DTP) to detect the formation of coenzyme A (CoA-SH) at 324 nm (ε = 19800 M^{-1} cm^{-1}). A typical reaction mix contained 50 mM HEPES (pH 7.5), 50 mM NaCl, 10 mM $MgCl_2$, 1 mM 3-[(3-cholamidopropyl)dimethylammonio]-1-propanesulfonate hydrate (CHAPS), 400 μM DTP, 100 μM Ac-CoA, and 200 μM GlcN-1P. Reactions were initiated by the addition of the enzyme, typically at a final concentration of 5 nM. Kinetic parameters for GlmU acetyltransferase were determined by measuring initial velocities at varying concentrations of either Ac-CoA or GlcN-1P and a constant, saturating concentration of the co-substrate.

Measurement of Uridylyltransferase Enzymatic Activity. Initial velocities for the forward uridylyltransferase reaction of GlmU were performed at 30 °C using inorganic pyrophosphatase and two different assay methodologies to detect the formation of pyrophosphate and subsequently inorganic phosphate (P_i). The two assay methodologies have both been previously described and make up an enzyme-coupled system for detecting the formation of free phosphate in solution through the formation of the fluorescent product resorufin,[34] and a 7-(diethylamino)-3-({[(2-maleimidyl)ethyl]-amino}carbonyl)coumarin (MDCC)-labeled P_i binding protein (MDCC-PBP).[35] The enzyme-coupled phosphate detection assay relies on coupling phosphate generation to purine nucleoside phosphorylase, xanthine oxidase, and horseradish peroxidase. A typical reaction mix contained 50 mM HEPES (pH 7.5), 50 mM NaCl, 10 mM $MgCl_2$, 1 mM CHAPS, 1.5 mM inosine, 50 μM Amplex Red, 0.02 IU/mL purine nucleoside phosphorylase (PNP), 0.4 IU/mL xanthine oxidase (XOD), 1 IU/mL horseradish peroxidase (type XII) (HRP), 20 μM UTP, and 50 μM GlcNAc-1P. The fluorescence signal obtained was measured using a Tecan Infinite M1000 Pro microplate reader using 530 nm for excitation and 590 nm for emission. Reactions were initiated by the addition of enzyme, typically 5 nM GlmU and 1 IU/mL pyrophosphatase (final concentrations).

The PBP detection assay relies on binding P_i, which causes a conformational change in the biosensor, alleviating fluorophore quenching, leading to an increase in fluorescence intensity. A typical reaction mix contained 50 mM HEPES (pH 7.5), 50 mM NaCl, 10 mM $MgCl_2$, 1 mM CHAPS, 15 μM PBP, 20 μM UTP, and 50 μM GlcNAc-1P. The fluorescence signal obtained was measured using a Tecan Infinite M1000 Pro microplate reader exciting the MDCC fluorophore of PBP at 425 nm and measuring fluorescence emission at 474 nm. Reactions were initiated by the addition of enzyme, typically 2.5 nM GlmU and 1 IU/mL pyrophosphatase (final concentrations).

Kinetic parameters for GlmU uridylyltransferase were determined by measuring initial velocities at varying concentrations of either UTP or GlcNAc-1P and a constant, saturating concentration of the co-substrate. The enzyme-coupled P_i detection assay was used to monitor the competition of GlmU acetyltransferase CoA-SH with GlcN-1P. Initial velocities were measured for titrations of CoA-SH at several fixed concentrations of GlcN-1P. The PBP biosensor assay was used to monitor the competition of GlmU acetyltransferase

CoA-SH with Ac-CoA. Initial velocities were measured for titrations of CoA-SH at several fixed concentrations of Ac-CoA.

^{1}H NMR Spectroscopy and pH Titration. NMR measurements were performed at 21.5 °C, on a Bruker Avance 600 MHz instrument equipped with a 5 mm TCI cryoprobe. At each pH value, one-dimensional ^{1}H NOESY[36] and ^{1}H^{13}C HSQC[37] spectra were acquired on a 40 mM natural abundance GlcN-1P sample in 100 mM KCl and a 93% H_2O/7% D_2O solution. The solution contained 2 mM formate, 2 mM imidazole, 2 mM Tris, and 2 mM piperazine as internal pH indicators and 0.2 mM DSS for ^{1}H chemical shift internal referencing according to Baryshnikova et al.[38]

The pH titration was performed using a cross-titration method in which aliquots of the two initial samples at pH 5.6 and 11.5 were reciprocally transferred between samples to achieve intermediate pH values. Spectra were acquired for each point to monitor chemical shift changes of both GlcN-1P and pH indicator protons. To determine pH values at each point of the titration accurately, the chemical shifts of the pH indicators were referenced to calibration curves previously acquired at the same temperature, according to the methods described by Oregioni et al.[39]

CH(1)-PO_4H_2 and CH(2)-NH_3^+ protons of GlcN-1P were preliminary assigned at pH 5.6 to signals at 5.64 and 3.32 ppm, respectively, using a two-dimensional COSY experiment,[40] and their chemical shift changes with pH were monitored on the assumption that they, in particular CH(2)-NH_3^+, would reflect the amino group ionization state in the measured pH range.

Inhibition Studies. To determine the concentration of inhibitor necessary to inhibit 50% of GlmU activity (IC_{50}), assays were performed in the presence of various concentrations of inhibitor, at fixed saturating concentrations of both substrates and $MgCl_2$. To determine inhibition constants (K_{ii} and K_{is}) and inhibition patterns, GlmU activity was studied in the presence of variable concentrations of one substrate and inhibitor, at fixed saturating concentrations of the co-substrate and $MgCl_2$.

pH–Rate Studies. The pH dependence of $V/K_{GlcN-1P}$ (k_{cat}/K_m) and V (k_{cat}) was determined by varying the concentration of GlcN-1P at a fixed, saturating concentration of Ac-CoA. The pH dependence of V/K_{Ac-CoA} (k_{cat}/K_m) and V (k_{cat}) was determined by varying the concentration of Ac-CoA at a fixed, saturating concentration of GlcN-1P. The pH dependence of GlmU H374A $V/K_{GlcN-1P}$ (k_{cat}/K_m) and V (k_{cat}) was determined by varying the concentration of GlcN-1P at a fixed, saturating concentration of Ac-CoA. In parallel, to control for the GlmU H374A studies, GlmU wild-type $V/K_{GlcN-1P}$ (k_{cat}/K_m) and V (k_{cat}) were determined by varying the concentration of GlcN-1P at a fixed, saturating concentration of Ac-CoA. All pH–rate studies were conducted in the following assay buffer that has previously been shown to buffer between pH 6 and 10, while maintaining a constant ionic strength: 50 mM 2-(N-morpholino)ethanesulfonic acid (MES), 50 mM HEPES, 100 mM ethanolamine, 10 mM $MgCl_2$, and 1 mM CHAPS.[41]

Differential Scanning Fluorimetry. Protein unfolding was monitored by SYPRO Orange (Fisher Scientific) fluorescence measurements on a Roche LightCycler 480 II RT-PCR machine, using 384-well microplates (white Accuflow Roche 480 plates), with filters to excite at 465 nm and measure emission at 580 nm as the temperature was continuously increased at a ramp rate of 0.11 °C/s. A typical experiment mix contained 25 mM HEPES (pH 7.5), 50 mM NaCl, 10 mM $MgCl_2$, 1 mM CHAPS, and 10% SYPRO Orange. Potential

binding partners were typically titrated in the presence of a fixed GlmU concentration of 2 μM. Differential scanning fluorimetry was also utilized to monitor protein stability over a pH range of 6–10. The methods for this can be found in the Supporting Information.

Solvent Kinetic Isotope Effects. SKIEs on V and V/K_{Ac-CoA} were determined in water (H_2O)- or 100% deuterium oxide (D_2O)-containing assay buffer, comprising 50 mM MES, 50 mM HEPES, 100 mM ethanolamine, 10 mM $MgCl_2$, and 1 mM CHAPS, in the presence of saturating concentrations of GlcN-1P at pL 8. Solvent KIEs on V and $V/K_{GlcN-1P}$ were determined in H_2O- or 100% D_2O-containing buffer, comprising 50 mM MES, 50 mM HEPES, 100 mM ethanolamine, 10 mM $MgCl_2$, and 1 mM CHAPS, in the presence of saturating concentrations of Ac-CoA at pL 8. Viscosity effects on V and V/K were evaluated by comparing rates obtained in H_2O- or 9% (w/w) glycerol-containing buffer, comprising 50 mM MES, 50 mM HEPES, 100 mM ethanolamine, 10 mM $MgCl_2$, and 1 mM CHAPS at pH 8. The use of 9% glycerol mimics the viscosity increase caused by the use of D_2O ($\eta_r = 1.24$).[42]

Crystallization, Data Collection, and Refinement of GlmU Bound to Glc-1P and Ac-CoA. To grow GlmU crystals, the protein solution was concentrated to 11 mg/mL. The apo GlmU was crystallized at 20 °C using the sitting-drop vapor diffusion method. Sitting drops of 1 μL consisted of a 1:1 (v/v) mixture of protein and a well solution containing 0.05 M ADA (pH 6.8), 5.7% PEG 550 MME, and 32.1% PEG 200. Crystals appeared after 12 h and reached their maximum size after 2 days (100 μm × 100 μm × 40 μm). Crystals were then soaked for 5 min in a solution containing 10 mM Glc-1P, 10 mM Ac-CoA, 0.05 M ADA (pH 6.8), 8% PEG 550 MME, and 35% PEG 200. Crystals were directly flash-frozen in liquid nitrogen, and X-ray data sets were collected at 100 K at the I03 beamline of the Diamond Light Source Synchrotron (Oxford, U.K., mx13775-39).

Data collection and refinement statistics are summarized in Table S4. The data set was indexed, scaled, and merged with xia2.[43] Molecular replacement was achieved by using the atomic coordinates of *M. tuberculosis* GlmU from PDB entry 4G87[44] in PHASER.[45] Refinement was performed by using Phenix,[46] model building in COOT,[47] and model validation PRO-CHECK,[48] and figures were prepared using the graphics program PYMOL.[49] The asymmetric unit contains one chain of GlmU. The difference electron density map covering GlmU shows unambiguous density for Glc-1P and Ac-CoA. The atomic coordinates and structure factors have been deposited in the PDB with accession codes 6GE9.

Data Analysis. All initial rate data were fitted using either SigmaPlot 12.5 or Grafit 7.0.2. Individual saturation curves were fitted to eq 1

$$v = VA/(A + K) \tag{1}$$

where V is the maximal velocity, A is the substrate concentration, and K is the Michaelis constant for the substrate (K_m). Individual saturating curves showing linear substrate inhibition were fitted to eq 2

$$v = VA/[K + A(A^2/K_i)] \tag{2}$$

where K_i is the apparent inhibition constant for substrate A. Data showing an intersecting initial velocity pattern on double-reciprocal plots were fitted to eq 3

$$v = VAB/(K_{ia}K_B + K_A B + K_B A + AB) \tag{3}$$

where A and B are the concentrations of the substrates and K_A and K_B are the Michaelis constants. Inhibition data showing linear, competitive, noncompetitive, or uncompetitive patterns in double-reciprocal plots were fitted to eqs 4–6

$$v = VA/[K(1 + I/K_{is}) + A] \tag{4}$$

$$v = VA/[K(1 + I/K_{is}) + A(1 + I/K_{ii})] \tag{5}$$

$$v = VA/[K + A(1 + I/K_{ii})] \tag{6}$$

where I is the inhibitor concentration and K_{is} and K_{ii} are the slope and intercept inhibition constants, respectively. Inhibition data, recorded under concentrations equivalent to K of substrates and variable concentrations of inhibitors, were fitted to eq 7

$$v = v_0/[1 + (I/IC_{50})^{n_H} + D] \tag{7}$$

where v is the rate in the presence of the inhibitor at concentration I, v_0 is the rate without the inhibitor, IC_{50} is the concentration of the inhibitor that gives 50% inhibition, n_H is the Hill coefficient, and D is the assay background. pH profile data were fitted to eq 8 for one basic ionizable group, eq 9 for two nonresolvable acidic ionizable groups, eq 10 for two acidic nonresolvable and two basic nonresolvable ionizable groups, and eq 11 for two acidic nonresolvable and one basic ionizable group

$$v = C/(1 + H/K_a) \tag{8}$$

$$v = C/(1 + H^2/K_a^2) \tag{9}$$

$$v = C/(1 + H^2/K_a^2 + K_b^2/H^2) \tag{10}$$

$$v = C/(1 + H^2/K_a + K_b/H) \tag{11}$$

where C is the pH-independent plateau value, H is the hydrogen ion concentration, and K_a and K_b are the acidic and basic pK_a constants, respectively, for the ionizable groups. Solvent kinetic isotope effects were fitted to eqs 12–14 for isotope effects on V only, V/K only, and both V and V/K, respectively

$$v = VA/[K + A(1 + F_i E_V)] \tag{12}$$

$$v = VA/[K(1 + F_i E_V/K) + A] \tag{13}$$

$$v = VA/[K(1 + F_i E_{V/K}) + A(1 + F_i E_V)] \tag{14}$$

where F_i is the fraction of the isotopic label and E_V and $E_{V/K}$ are the isotope effects minus one on V and V/K, respectively. Data from differential scanning fluorimetry thermal melting experiments were fitted to eq 15

$$y = LL + (UL - LL)/[1 + \exp(T_m - X/E)] \tag{15}$$

where LL and UL are the minimum and maximum intensities, respectively, X is the temperature, E is the slope of the curve, and T_m is the melting point. Plots of the change in T_m (ΔT_m) versus ligand concentration were fitted to eq 16

$$\Delta T_m = \Delta T_{m,max} A/(K_d + A) + D \tag{16}$$

where A is the ligand being titrated, K_d is its apparent dissociation constant, D is the assay background, and $\Delta T_{m,max}$ is the maximum possible T_m change. The pH dependence of ^{1}H GlcN-1P chemical shifts was fitted to eq 17

$$\delta_{peak} = \delta_{HA} + [\Delta\delta/1 + 10^{n_H(pH - pK_a')}] \tag{17}$$

where δ_{peak} is the peak chemical shift, δ_{HA} is the chemical shift of the protonated form, and $\Delta\delta$ is the difference between δ_{HA} and the shift of the deprotonated form. Errors were propagated as described by Skoog and West for indeterminate errors.[50]

■ RESULTS

Divalent Metal Activation. Preliminary protein purification experiments and subsequent initial enzymatic characterization experiments revealed a dependence of GlmU acetyltransferase activity on Mg^{2+}. This metal ion dependence manifested itself as a lag in the acetyltransferase progress curves (Figure 1). Further investigation demonstrated that this
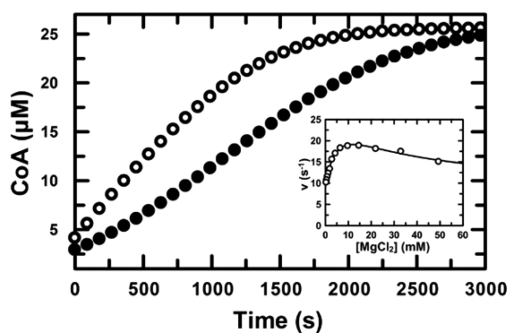

Figure 1. Progress curves of the GlmU acetyltransferase reaction using the DTP absorbance assay detailed in Materials and Methods. The change in DTP OD_{324} was monitored every 10 s and then converted to the concentration of CoA formed using the molar absorption coefficient of 4-thiopyridone (4-TP) and the Beer−Lambert law. The data for GlmU purified in the presence or absence of 10 mM $MgCl_2$ are represented by either empty or filled circles, respectively. The inset shows the determination of the GlmU acetyltransferase Mg^{2+} K_{act}, which is defined as the concentration of metal ion required for half-maximal activity at saturating substrate concentrations (the concentrations of Ac-CoA and GlcN-1P were both 2 mM). Symbols represent experimental data, and solid lines are fits of the data to eq 2. Mn^{2+} and Ca^{2+} were activators of GlmU acetyltransferase activity (see the Supporting Information), while Co^{2+}, Ni^{2+}, and Zn^{2+} were not activators.

nonlinear acetyltransferase activity was reversed via prolonged incubation with 10 mM Mg^{2+} at 4 °C (data not shown). GlmU was incubated with EDTA overnight, followed by dialysis, along with a non-EDTA incubation control, in an attempt to remove any tightly bound divalent metal ions. Subsequent acetyltransferase activity assays in the presence and absence of 10 mM Mg^{2+} indicated that there was little difference between the EDTA-incubated, dialysis control and the nontreated enzyme. A significant difference in acetyltransferase activity, while still initially nonlinear, was observed between GlmU stocks in the presence and absence of 10 mM Mg^{2+}, indicating that there is an absolute divalent metal ion requirement for optimal activity (data not shown). To characterize the apparent activation of GlmU acetyltransferase activity, Mg^{2+} was titrated to determine a $K_{act,Mg^{2+}}$ of 5.7 ± 1.3 mM, with optimal catalysis achieved at a Mg^{2+} concentration of 10 mM (Figure 1). Further studies were performed to characterize the divalent metal ion specificity of GlmU for optimal acetyltransferase activity (all as chlorine salts), with Mn^{2+} and Ca^{2+} identified as possible alternatives (Table S1). The dependence of GlmU acetyltransferase kinetic parameters on Mg^{2+} was investigated, but only modest changes

were observed for both Ac-CoA and GlcN-1P at high metal ion concentrations (Figure S2). Ultimately, a further protein purification was performed, ensuring that 10 mM $MgCl_2$ was present for all steps, which resulted in eradication of the nonlinear GlmU acetyltransferase progress curves (Figure 1). To ensure optimal GlmU acetyltransferase activity, all further enzyme assays were performed with enzyme purified in buffer containing 10 mM $MgCl_2$ throughout the purification process and reactions included 10 mM $MgCl_2$.

Initial Velocity Studies. To characterize the kinetic mechanism, initial velocity studies were performed by varying Ac-CoA concentrations at various fixed GlcN-1P concentrations. Intersecting patterns on double-reciprocal plots were generated (Figure 2), consistent with GlmU following a
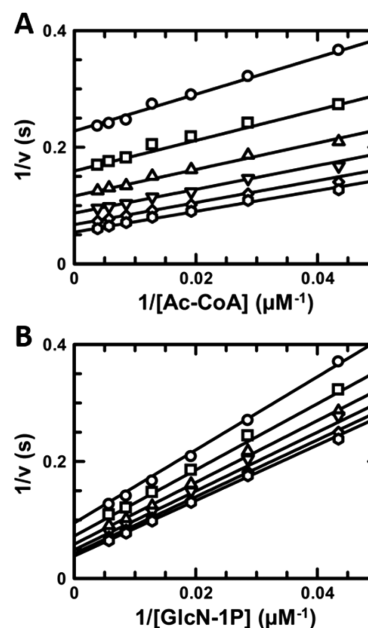

Figure 2. GlmU initial velocity patterns. Double-reciprocal plot of GlmU initial rates (A) at varying concentrations of Ac-CoA (>20 μM) and several fixed concentrations of GlcN-1P [23 μM (○), 35 μM (□), 52 μM (△), 78 μM (▽), 117 μM (◇), and 175 μM (◯)] and (B) at varying concentrations of GlcN-1P (>20 μM) and several fixed concentrations of Ac-CoA [23 μM (○), 35 μM (□), 52 μM (△), 78 μM (▽), 117 μM (◇), and 175 μM (◯)]. Symbols represent experimental data, and solid lines are fits of the data to eq 3.

sequential bi-bi kinetic mechanism. Steady-state kinetic parameters for GlmU acetyltransferase activity, $K_{m,Ac-CoA}$, $K_{m,GlcN-1P}$, and k_{cat}, were obtained by fitting these data to eq 3, and these results are presented in the legend of Figure 2. Secondary replots of the slope and intercept values determined from the initial velocity patterns in Figure 2 demonstrate that a rapid equilibrium ordered mechanism is unlikely, as the slope replot for GlcN-1P does not intersect at 0 (Figure S3). Attempts to fit the data shown in Figure 2 to an equation describing a ping-pong mechanism yielded very large errors.

Substrate Specificity. Kinetic parameters were determined from saturation curves and fitting to eq 1, for a range of GlcN-1P and Ac-CoA analogues (Table 1). No acetyltransferase activity was detected, at a concentration of ≤10 mM, for the following GlcN-1P analogues: galactosamine 1-phosphate, glucosamine, galactosamine, mannosamine, mannose 1-phosphate, mannose 6-phosphate, N-acetyl-glucosamine (GlcNAc), N-acetyl-galactosamine, N-acetyl-mannosamine, glucose 1-

Table 1. Steady-State Kinetic Parameters for GlmU[a]

varied substrate	fixed substrate	K_m (μM)[b]	k_{cat} (s^{-1})[b]	k_{cat}/K_m (M^{-1} s^{-1})[b]	K_d (μM)[b]
		Canonical Order			
Ac-CoA	GlcN-1P	250 ± 8	28 ± 1	(1.1 ± 0.6) × 10^5	250 ± 25
GlcN-1P	Ac-CoA	290 ± 31	28 ± 1	(9.7 ± 1.6) × 10^4	ND
UTP	GlcNAc-1P	8 ± 0.8	120 ± 3	(1.5 ± 0.38) × 10^7	ND
GlcNAc-1P	UTP	30 ± 5	100 ± 4	(3.2 ± 0.8) × 10^6	ND
		Reverse Order			
Ac-CoA	UDP-GlcN[c]	40 ± 7	0.27 ± 0.02	(7.5 ± 2.9) × 10^3	250 ± 25
UDP-GlcN	Ac-CoA	9700 ± 600	2.04 ± 0.06	(2.2 ± 1.7) × 10^2	ND
UTP	GlcN-1P	–	–	–	ND
GlcN-1P	UTP	–	–	–	ND
		Substrate Analogues			
AAc-CoA	GlcN-1P	1800 ± 200	0.5 ± 0.27	(2.8 ± 15) × 10^2	ND
GlcN-1P	AAc-CoA[c]	16 ± 6	0.13 ± 0.01	(8.1 ± 0.5) × 10^3	ND
Pro-CoA	GlcN-1P[c]	60 ± 2	0.5 ± 0.01	(8.3 ± 5) × 10^3	500 ± 100
GlcN-1P	Pro-CoA	980 ± 110	0.5 ± 0.01	(5.1 ± 0.9) × 10^2	ND
Suc-CoA	GlcN-1P[c]	1100 ± 100	0.9 ± 0.26	(8.2 ± 30) × 10^2	ND
GlcN-1P	Suc-CoA	–	–	–	ND

[a]Reactions performed at pH 7.5 and 30 °C. [b]Values are means of at least three experiments ± the standard error obtained upon fitting the data to the appropriate equation. [c]Nonsaturating concentrations of the fixed substrate used: 800 μM UDP-GlcN, 1 mM AAc-CoA, and 3 mM GlcN-1P. All data were fit to eq 1. The following analogues were tested but were not substrates of GlmU acetyltransferase (no activity at ≤10 mM): Dethio-CoA, Bu-CoA, Eth-CoA, IsoBu-CoA, Mlo-CoA, Cro-CoA, GlcNAc, Glc-1P, GlcN-6P, GalN-1P, galactose 1-phosphate, galactosamine, mannosamine, mannose 1-phosphate, *N*-acetyl-galactosamine, *N*-acetyl-mannosamine, glucose 6-phosphate, and mannose 6-phosphate.

phosphate (Glc-1P), glucosamine 6-phosphate (GlcN-6P), glucose 6-phosphate, and galactose 6-phosphate. Inhibition was observed with some of these GlcN-1P analogues (see the next section). UDP-glucosamine (UDP-GlcN) was the only GlcN-1P analogue tested that is a substrate of GlmU acetyltransferase (Figure 3).
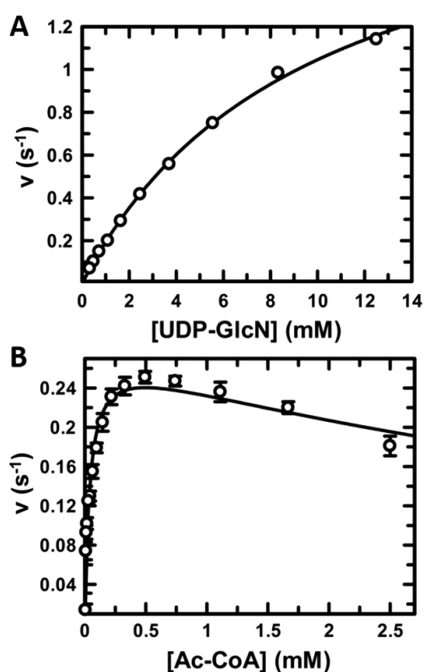

Figure 3. GlmU acetyltransferase steady-state kinetics utilizing UDP-GlcN as a second substrate. (A) Titration of UDP-GlcN at a saturating concentration of Ac-CoA. Symbols represent experimental data, and solid lines are fits of the data to eq 1. (B) Titration of Ac-CoA at a nonsaturating concentration of UDP-GlcN (800 μM). Symbols represent experimental data, and solid lines are fits of the data to eq 2.

GlmU acyltransferase activity was not detected, at a concentration of ≤10 mM, for the following acyl-CoAs: ethyl-CoA (Eth-CoA), butyryl-CoA (Bu-CoA), isobutyryl-CoA (IsoBu-CoA), malonyl-CoA (Mlo-CoA), crotonyl-CoA (Cro-CoA), stearoyl-CoA, HMG-CoA, palmitoyl-CoA, and glutaryl-CoA. Although these analogues were not substrates, some were identified as inhibitors and will be presented in the next section. The Ac-CoA analogues identified as substrates were acetoacetyl-CoA (AAc-CoA), *n*-propionyl-CoA (Pro-CoA), and succinyl-CoA (Suc-CoA).

A number of acyl-CoAs, along with CoA-SH (Figure S6) and two GlcN-1P analogues, were identified as not being acetyltransferase substrates but were inhibitors (Table 2).

Product and Dead-End Inhibition Studies. Product inhibition was used to investigate the order of binding of substrate to and release of product from the GlmU acetyltransferase domain. The results are listed in Table 3. Overall, the results are consistent with GlmU following an ordered sequential mechanism. Given that CoA-SH is competitive versus Ac-CoA and noncompetitive versus GlcN-1P a sequential ordered mechanism is likely, with Ac-CoA binding first followed by GlcN-1P. No inhibition was observed when GlcNAc-1P was tested versus Ac-CoA or GlcN-1P, at saturating and several subsaturating concentrations of the respective co-substrate. Although these results would support an equilibrium ordered kinetic mechanism, with GlcNAc-1P as the first product to dissociate followed by CoA-SH as illustrated in Scheme 2, other observations are inconsistent with an equilibrium mechanism but support a steady-state kinetic mechanism (see above and below).

To further probe the kinetic mechanism for the GlmU acetyltransferase, dead-end inhibition experiments were performed (Table 2). The dead-end inhibitors selected for these studies were Bu-CoA and Glc-1P, which were shown to inhibit GlmU acetyltransferase in a partial mutually exclusive manner; i.e., binding of both inhibitors is disfavored by ~3-fold (Figure S4). Taken together, the results were in agreement with GlmU

Table 2. Substrate Analogue and Product Inhibition Parameters for GlmU[a]

inhibitor	IC_{50} (mM)[b,c]	n_H[b,c]	K_d (mM)[c]
CoA-SH	0.3 ± 0.01	0.9 ± 0.1	0.7 ± 0.13
Eth-CoA[d]	ND		ND
Bu-CoA	1 ± 0.03	1.2 ± 0.1	3.8 ± 0.8
IsoBu-CoA	2 ± 0.21	1.5 ± 0.2	ND
Mlo-CoA	2 ± 0.59	1.1 ± 0.6	ND
Cro-CoA	1 ± 0.15	1.2 ± 0.1	ND
GlcNAc[d]	ND	ND	ND
Glc-1P	5 ± 0.65	1.0 ± 0.1	ND
GlcN-6P	10 ± 0.89	1.1 ± 0.1	ND
GalN-1P	120 ± 30	1.1 ± 0.1	ND

[a]Reactions performed at pH 7.5 and 30 °C. [b]Reactions were performed using K_m concentrations of Ac-CoA and GlcN-1P, competitors titrated from 20 μM. [c]Values are means of at least three experiments ± the standard error obtained upon fitting the data to the appropriate equation. [d]Ligands that show dependent inhibition but at the highest tested concentration do not fully inhibit GlmU acetyltransferase activity. The following analogues were tested but were not inhibitors of GlmU acetyltransferase (no inhibition at ≤10 mM): GlcNAc-1P, Dethio-CoA, galactose 1-phosphate, galactosamine, mannosamine, mannose 1-phosphate, N-acetyl-galactosamine, N-acetyl-mannosamine, glucose 6-phosphate, and mannose 6-phosphate.

acetyltransferase following an ordered, sequential mechanism. Competitive inhibition patterns were obtained for Bu-CoA versus Ac-CoA or versus GlcN-1P. These data are indicative of Bu-CoA competing for binding to the free enzyme and also preventing GlcN-1P from binding, likely by steric hindrance. As expected, competitive inhibition was also observed for the Glc-1P versus GlcN-1P inhibition pattern. Glc-1P inhibition versus Ac-CoA is uncompetitive, which indicates that Glc-1P binds to the E:CoA-SH complex, and not to free or Ac-CoA-bound enzyme. This was confirmed at subsaturating concentrations of the co-substrate (Figure S7). These findings are incorporated into Scheme 2, which illustrates the proposed ordered sequential mechanism for the GlmU acetyltransferase reaction. Additionally, the equilibrium constants for the dissociation of Ac-CoA, Bu-CoA, CoA-SH, GlcN-1P, and Glc-1P from GlmU were obtained by using differential scanning fluorimetry (DSF) to measure the change in enzyme melting temperature (T_m) at different ligand concentrations. From these studies, we determined K_d values, which are listed in Table 1 and Table S2. Dissociation constants for dissociation of GlcN-1P and Glc-1P from GlmU could not be determined without Ac-CoA or an

analogue present; however, in the presence of high concentrations of the second substrate, the K_d values for the complex could be determined, which are given in Table S2 and Figure S5.

pH−Rate Studies. We investigated the effect of pH on GlmU acetyltransferase kinetic parameters, to assess the role of general acid−base chemistry in catalysis and substrate recognition, from pH 6.00 to 10.00 (Figure 4). Initially, GlmU activity was tested at all pH values used in these experiments to confirm that no loss of activity was observed (data not shown). Additionally, no significant changes in protein stability were observed in the pH range tested (Table S3). Furthermore, GlmU acetyltransferase progress plots were linear for several minutes under all pH conditions utilized, both when the experiment was performed with a minimal enzyme incubation and after an extended 2 h preincubation at the test pH, prior to assay initiation (data not shown). The pH dependence of k_{cat} reveals both acid- and base-assisted catalysis. The bell-shaped curve of k_{cat} versus pH has slopes of +2 and −2 in the acidic and basic regions, respectively. These data were best fitted to eq 10, describing the involvement of two acidic nonresolvable and two basic nonresolvable ionizable groups, which must be deprotonated and protonated for maximal activity, respectively. Fitting to eq 10 yields pK_a values of 6.7 ± 0.1 and 9.0 ± 0.1 for the groups that need to be deprotonated (general base) and protonated (general acid), respectively, for maximal activity. Similarly, the plot of pH versus log $k_{cat}/K_{m,GlcN-1P}$ was bell-shaped, with slopes of +2 and −2 in the acidic and basic regions, respectively. These data were best fitted to eq 10, describing the role of two acidic nonresolvable and two basic nonresolvable ionizable groups, which must be deprotonated and protonated, respectively, for maximal activity. Fitting to eq 10 yields pK_a values of 7.5 ± 0.1 and 9.1 ± 0.1 for the acidic and basic groups, respectively. Finally, the bell-shaped plot of pH versus log $k_{cat}/K_{m,Ac-CoA}$ has slopes of +2 at low pH and −1 at high pH. Fitting of these data to an equation describing the role of two nonresolvable acidic groups and one basic group (eq 11), which must be deprotonated and protonated for maximal activity, respectively, yields pK_a values of 6.6 ± 0.1 and 8.1 ± 0.1 for the two acidic groups and one basic group, respectively. The pH−rate profile of GlmU H374A was obtained to confirm its role as the general base responsible for deprotonation of the GlcN-1P amino group. GlmU H374A is significantly slower than wild-type GlmU, displaying a pH-independent plateau that is approximately 3 orders of magnitude lower than that of wild-type GlmU (Figure 5).

Table 3. Product Inhibition Patterns and Inhibition Constants for GlmU[a]

varied substrate	inhibitor	fixed substrate	inhibition pattern[c]	K_{is} (mM)	K_{ii} (mM)
		Product Inhibition			
GlcN-1P	CoA-SH	10K_m Ac-CoA	NC	0.21 ± 0.086	0.8 ± 0.09
Ac-CoA	CoA-SH	10K_m GlcN-1P	C	0.15 ± 0.015	
GlcN-1P	GlcNAc-1P	0.5−10K_m Ac-CoA	NI		
Ac-CoA	GlcNAc-1P	0.5−10K_m GlcN-1P	NI		
		Dead-End Inhibition			
GlcN-1P	Glc-1P	10K_m Ac-CoA	C	4.1 ± 0.6	
Ac-CoA	Glc-1P	0.5−10K_m GlcN-1P[b]	UC		11.56 ± 0.9
GlcN-1P	Bu-CoA	10K_m Ac-CoA	C	1.2 ± 0.2	
Ac-CoA	Bu-CoA	10K_m GlcN-1P	C	0.35 ± 0.03	

[a]Reactions performed at pH 7.5 and 30 °C. [b]Range of GlcN-1P concentrations used from 0.5K_m to 10K_m. [c]Abbreviations: NC, noncompetitive; C, competitive; UC, uncompetitive; NI, no inhibition.
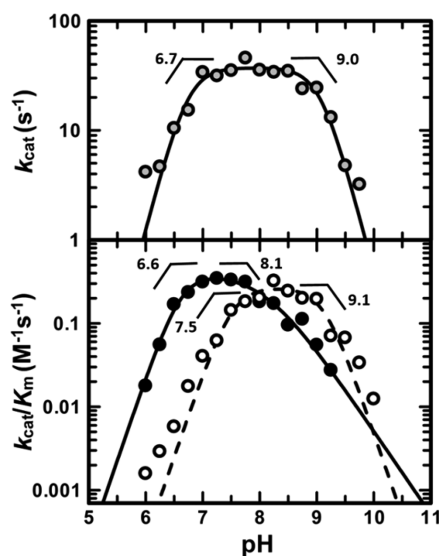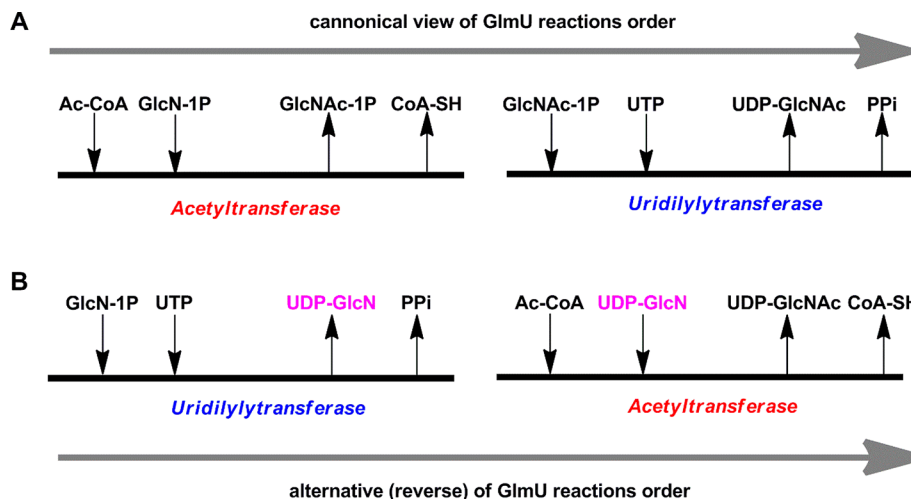
Scheme 2. GlmU Alternative Reaction Order

A cannonical view of GlmU reactions order

Ac-CoA GlcN-1P   GlcNAc-1P CoA-SH   GlcNAc-1P UTP   UDP-GlcNAc PPi

Acetyltransferase   *Uridilyltransferase*

B GlcN-1P UTP   UDP-GlcN PPi   Ac-CoA UDP-GlcN   UDP-GlcNAc CoA-SH

Uridilyltransferase   *Acetyltransferase*

alternative (reverse) of GlmU reactions order

Figure 4. pH dependence of GlmU kinetic parameters. The k_{cat} and K_m values were determined at each pH by varying concentration of one substrate at a fixed, saturating concentration of the second substrate. The k_{cat} data are means of the Ac-CoA and GlcN-1P values and are shown as gray filled circles, and the best fit of the data, to eq 10, is represented by the solid line. Ac-CoA k_{cat}/K_m data are shown as filled circles, and the best fit of the data, to eq 11, is represented by the solid line. The GlcN-1P k_{cat}/K_m data are shown as open circles, and the best fit of the data, to eq 10, is represented by the dashed line.

Figure 5. pH dependence of GlmU and GlmU H374A acetyltransferase kinetic parameters. The k_{cat} and K_m values were determined at each pH by varying the concentration of GlcN-1P at a fixed, saturating concentration of Ac-CoA. The GlcN-1P data relating to wild-type GlmU k_{cat} and k_{cat}/K_m data are represented by black filled circles, and the best fit of the data, to eq 10, is represented by the solid line. The GlcN-1P data relating to GlmU H374A k_{cat} and k_{cat}/K_m data are represented by gray filled circles, and the best fit of the data, to eq 8, is represented by the solid line.

The pH dependence of k_{cat} reveals a single ionizable group that must be deprotonated for maximal activity (slope of +1). These data were best fitted to eq 8, describing the involvement of one basic ionizable group, which must be deprotonated for maximal activity. Fitting to eq 8 yields pK_a values of 8.2 ± 0.1 for this general base. Similarly, the plot of pH versus log $k_{cat}/K_{m,GlcN-1P}$ showed a single ionizable group (slope of +1), which was best fitted to eq 8, yielding a value of 9.7 ± 0.5 for the basic group. Further acetyltransfersae pH−rate profile data for wild-type GlmU were generated in parallel with the GlmU H374A study. This control study, utilizing GlcN-1P as the varied substrate, was best fitted to the equation for two nonresolvable acidic groups and one basic group (eq 11). Fitting the GlmU wild-type pH−rate profile data to eq 11 yields pK_a values for $k_{cat,GlcN-1P}$ of 6.4 ± 0.3 and 8.9 ± 0.3 and pK_a values for $k_{cat}/$
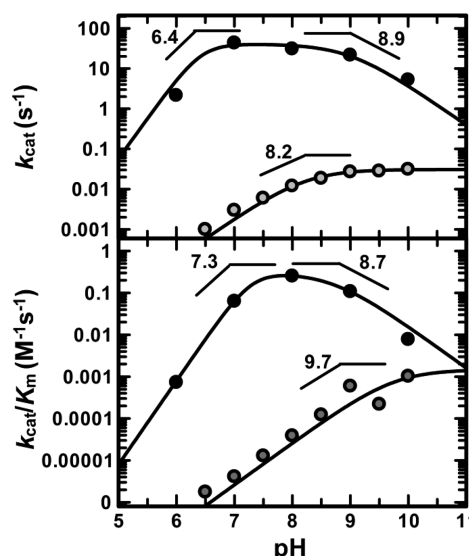
$K_{m,GlcN-1P}$ of 7.3 ± 0.02 and 8.7 ± 0.04 for the acidic and basic groups, respectively, in both cases.

Assessment of GlcN-1P Amino Group Ionization. To determine the pK value of the amine group of GlcN-1P under our experimental conditions, which is essential for further interpretation of the GlcN-1P pH−rate profile, we investigated the ionization state of GlcN-1P in solution. The NMR chemical shifts of two ^1H groups, $CH(2)-NH_3^+$ and $CH(1)-PO_4H_2$, were monitored over the pH range of 5.5−11.5 (Figure 6). The ^1H chemical shift of $CH(2)-NH_3^+$ was 3.33 ppm, while the ^1H chemical shift of $CH(1)-PO_4H_2$ was 5.65 ppm. These data were fitted to eq 17, which yielded a pK_a for NH_3^+ of 8.43 ± 0.01.

Solvent Kinetic Isotope Effects. SKIEs were determined in either 100% H_2O or 99.9% D_2O. Additionally, viscosity
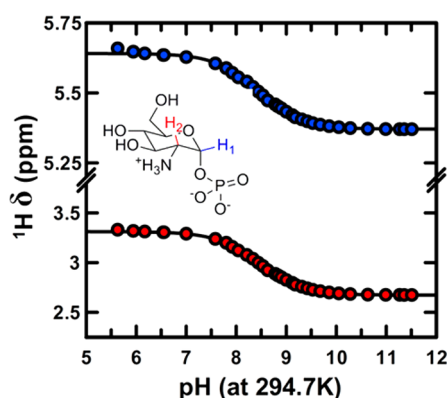
Figure 6. pH titration of GlcN-1P followed by NMR. Acidic and basic preparations of GlcN-1P were titrated to determine a pK_a for the protonated amine group. The ^1H peak intensities of $CH(2)$-NH_3^+ (experimental data represented by red filled circles) and $CH(1)$-PO_4H_2 (experimental data represented by dark blue filled circles) were monitored. The starting chemical shift for $CH(2)$-NH_3^+ was 3.33 ppm, while the starting chemical shift for $CH(1)$-PO_4H_2 was 5.65 ppm. The data were fitted to eq 17, and the best fit is represented by the solid line. The structure of GlcN-1P is given as the inset, and $CH(2)$-NH_3^+ and $CH(1)$-PO_4H_2 are colored red and blue, respectively.

controls were included using 9% glycerol as a viscogen to mimic the increased viscosity caused by using D_2O. A pL of 8 was selected as it corresponds to the plateau region of the pH profile, where the velocity is maximal and the variation due to changes in pH or pD is the smallest. GlcN-1P and Ac-CoA were tested as the variable substrates in the presence of fixed, saturating levels of the corresponding second substrate (Figure 7A,C, Table 4, and Figure S8). The GlcN-1P and Ac-CoA saturation curves determined in the presence of 9% glycerol acted as controls to show if effects of viscosity on initial rates associated with the use of D_2O instead of H_2O are present (Figure 7B,D).
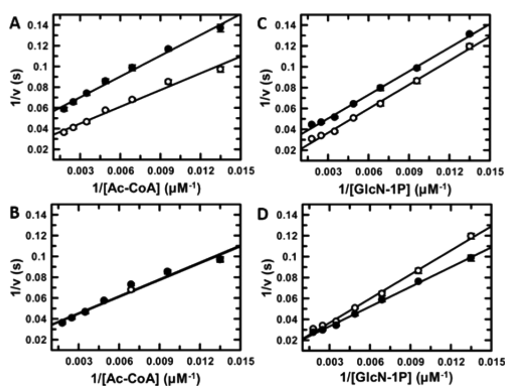

Figure 7. Solvent kinetic isotope effects for GlmU. For panels A and B, Ac-CoA was used as the varied substrate, with a saturating concentration of GlcN-1P. (A) The reaction mix contained either 0 (○) or 100 (●) atom % D_2O. (B) The reaction mix contained either 0 (○) or 9 (●) % glycerol. For panels C and D, GlcN-1P was used as the varied substrate, with a saturating concentration of Ac-CoA. (C) The reaction mix contained either 0 (○) or 100 (●) atom % D_2O. (D) The reaction mix contained either 0 (○) or 9 (●) % glycerol. The experimental data are represented by circles, and the best fit of the data is represented by the solid line. (A) Aata fitted to eq 14. (B) Data fitted to eq 14. (C) Data fitted to eq 12. (D) Data to fitted to eq 13.

Table 4. Solvent Kinetic Isotope Effects and Viscosity Controls for GlmU[a]

varied substrate	fixed substrate	^{D_2O}V	$^{D_2O}V/K$
	Solvent Kinetic Isotope Effect		
Ac-CoA	GlcN-1P	1.61 ± 0.03	1.36 ± 0.08
		1.61 ± 0.03	1.32 ± 0.1
GlcN-1P	Ac-CoA	1.59 ± 0.07	1
		1.55 ± 0.07	1
	Viscosity Effect[b]		
Ac-CoA	GlcN-1P	1	1
GlcN-1P	Ac-CoA	1	0.76 ± 0.08

[a]Solvent isotope effects were determined in assay buffer prepared in either 100% H_2O or 100% D_2O, at pH 8 and 30 °C. [b]Solvent isotope effect viscosity control using 9% glycerol in assay buffer as a viscogen.

Structure of GlmU in Complex with Ac-CoA and Glc-1P. To confirm and rationalize inhibition of GlmU acetyltransferase activity by the dead-end inhibitor, Glc-1P, we soaked apo-GlmU crystals in Ac-CoA and Glc-1P (Figure 8 and Table S4). This approach was successful and allowed us to determine the crystal structure of the E:Ac-CoA:Glc-1P complex (PDB ID 6GE9), to a resolution of 2.26 Å, uniquely, without the addition of the uridylyltransferase product UDP-GlcNAc, which had previously been postulated to be critical for stabilization of the E:Ac-CoA complex. The overall molecular structure of the E:Ac-CoA:Glc-1P complex is similar to that of the previously reported *M. tuberculosis* GlmU E:CoA-SH:GlcN-1P ternary complex; both complexes superimpose well with a root-mean-square deviation of 0.46 Å over 414 Cα atoms. The structure of the E:Ac-CoA:Glc-1P complex displays the conserved GlmU two-domain architecture, organized into a trimer formed around a 3-fold crystallographic symmetry (Figure 8A). Shown in Figure 8B is a close-up of the binding of Ac-CoA and Glc-1P in the acetyltransferase active site of GlmU, in addition to the orientation of a loop, which is positioned over the acyl thioester of Ac-CoA. This loop, which has been shown to be disordered in previous apo structures, brings Tyr398 into the proximity of Ac-CoA, allowing an interaction between its backbone carbonyl and nitrogen N4P of Ac-CoA.[32]

The binding of Glc-1P to GlmU (Figure 8C) is very similar to what has previously been reported for GlcN-1P[32] (Figure 8D). Glc-1P binds in a pocket that is proximal to the re face of the planar acetyl group of Ac-CoA and interacts with three basic residues (Arg344, Lys362, and Lys403) as well as the side chains of Asn397 and Tyr377. In addition, two hydrogen bonds are made with the side chain of Asn388 belonging to a second monomer. The interactions formed by Lys403 and Asn397 are a result of the ordering of the mobile loop upon Ac-CoA binding. An additional interaction enabled by stabilization of the disordered loop is contributed by the phenolic ring of Tyr398, which stacks with the hexose ring of Glc-1P (Figure S9).[51] Importantly, the Glc-1P 2-hydroxyl group forms two hydrogen bonds, one with Nε2 of the imidazole group of His374 and a second with the carbonyl group of the Ac-CoA acetyl group. Interestingly, the side chain of the acidic Glu360 forms a hydrogen bond with the basic residue His374. This interaction aligns the His374 side chain by restricting its rotation and polarizes the imidazole group by stabilizing its positive charge on Nδ1 (Figure S9). This interaction might be able to tune the pK_a of the imidazole allowing it to work as a general base.[52]
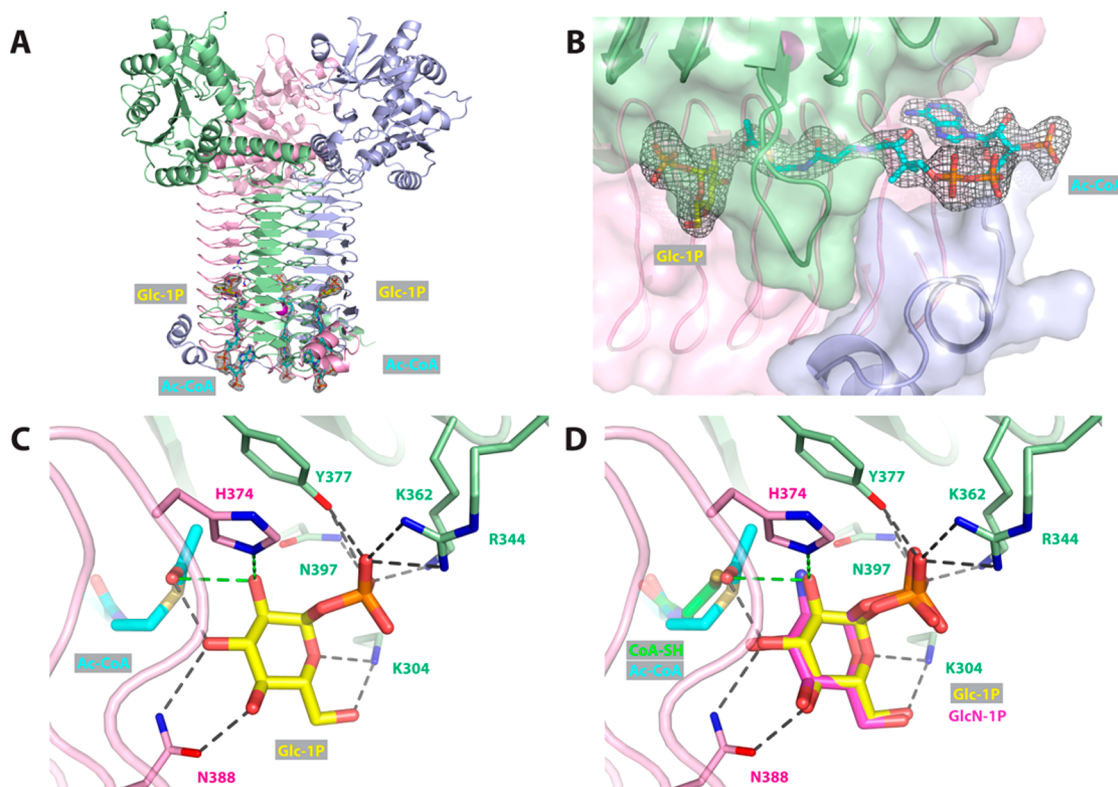
Figure 8. Structure of GlmU in complex with Glc-1P and Ac-CoA. (A) Overview of the GlmU trimeric assembly bound to Glc-1P and Ac-CoA. Each monomer is displayed in cartoon representation with Glc-1P and Ac-CoA shown as yellow and cyan sticks, respectively. The $F_o - F_c$ omit map contoured at 3σ is displayed around both ligands. (B) Close-up of Glc-1P and Ac-CoA ligands bound to GlmU. (C) Glc-1P binding site. For the sake of clarity, only the residues contributing to Glc-1P binding are displayed as sticks. The hydrogen bonds formed with Glc-1P atom O2 are colored green. (D) Same as panel C with GlcN-1P and CoA-SH from the crystal structure 3ST8 superimposed.

■ DISCUSSION

In this work, we present steady-state kinetics and binding data for *M. tuberculosis* GlmU, which together allow us to suggest a feasible kinetic and chemical mechanism for acetyl transfer by this bifunctional enzyme. Initially, we investigated the requirement and specificity of GlmU acetyltransferase for divalent metal ions, which was not previously characterized in any depth with any GlmU homologue, as divalent metals are usually not required cofactors in acetyl transfer reactions. A majority of studies of GlmU homologues published to date have used a fixed concentration of Mg^{2+}, in the range of 0.5−10 mM,[13,17,28,32] presumably based on the early work of Mengin-Lecreulx and van Heijenoort.[13] We demonstrate that the optimal concentration of Mg^{2+} for maximal GlmU acetyltransferase activity is 10 mM, and the $K_{act,Mg^{2+}}$ is 5.7 ± 1.3 mM. There is likely a tightly bound metal ion present from the protein purification process, which could not be removed by overnight incubation with EDTA and results in a background activity that can be observed in the inset of Figure 1. The metal ion specificity of GlmU for optimal acetyltransferase was explored with Ca^{2+} and Mn^{2+} identified as viable alternatives to Mg^{2+}. The dependence of GlmU acetyltransferase kinetic parameters on Mg^{2+} was investigated, and some effects on the GlcN-1P parameters were observed; however, these were only modest and likely not significant. To minimize the initial nonlinear acetyltransferase activity of GlmU, it was necessary to incubate protein with Mg^{2+} overnight or repurify the enzyme in the presence of 10 mM Mg^{2+}. Activation by divalent metal ions, specifically Mg^{2+}, Ca^{2+},

and Mn^{2+}, has previously been reported for the related *M. tuberculosis* enzyme tetrahydrodipicolinate *N*-succinyltransferase (DapD), which is a trimer in solution and a member of the LβH acyltransferase superfamily. Indeed, the divalent metal binding site is found in a similar position, at the trimer, 3-fold axis of symmetry in both enzymes. Finally, the same nonlinear acyltransferase activity was observed in the absence of added, activating divalent metal ions.[53] When these previous observations are taken into account, along with the findings from this study, it seems plausible to conclude that the divalent metal bound in GlmU plays a structural role, which only modestly impacts acetyl transfer. Importantly, no evidence of changes in oligomeric state have been observed (data not shown), and GlmU appears to be a trimer under all experimental conditions tested.

The magnitude of the measured kinetic parameters was similar to the magnitude of those previously determined for *M. tuberculosis* GlmU, as well as other orthologues, specifically $K_{m,Ac-CoA}$ and $K_{m,GlcN-1P}$, which were reported to be in the ranges of 200−400 and 60−360 μM, respectively.[28,32,54−56] Furthermore, the magnitude of the $K_{m,UTP}$ and $K_{m,GlcNAc-1P}$ parameters for the uridylyltransferase activity was similar to the magnitude of the reported values, which are 10−70 and 20−110 μM, respectively.[28,56] The k_{cat} values for both acetyltransferase and uridylyltransferase activities appear to be more variable, in the ranges of 50−1500 and 1−350 s^{-1}, respectively.[28,54,56] The reasons for these large differences in previously measured k_{cat} values are unclear but may partly be caused by the use of discontinuous assays in some studies, which inherently are associated with greater variabilities and

Scheme 3. Proposed Kinetic Mechanism for *M. tuberculosis* GlmU
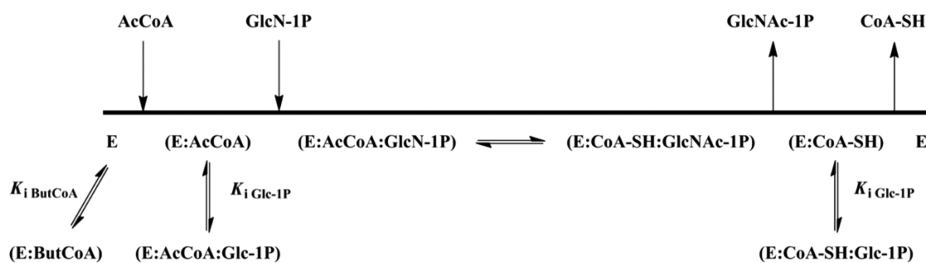
error. Nonetheless, the GlmU $k_{cat,acetyltransferase}$ is 28 s^{-1}, which is <2-fold lower than the reported range, and the GlmU $k_{cat,uridylyltransferase}$ is 110 s^{-1}, which is within the range of the reported values.

The substrate specificity for GlmU acetyltransferase was probed in this work with a variety of analogues of Ac-CoA and GlcN-1P. As previously reported for *E. coli* GlmU, there is some flexibility in the length of the acyl moiety that can be transferred from CoA to the amine group of GlcN-1P, with Pro-CoA and Suc-CoA being substrates that are roughly 10- and 100-fold less efficient, respectively [k_{cat}/K_m (Table 1)]. Although a three-carbon long acyl substrate is used, Bu-CoA (with four carbons) is no longer a substrate but is still able to bind GlmU and displays some inhibition. The acyl-CoAs, AAc-CoA and Suc-CoA, were both identified as substrates [low k_{cat}/K_m (Table 1)] but have thioester chain lengths similar to that of Bu-CoA. However, because of the CoA-SH detection methodology used to monitor the acetyltransferase reaction, these substrates could be hydrolyzed by GlmU.

The GlcN-1P substrate specificity is much more restricted than that of Ac-CoA, with only UDP-GlcN identified as an alternative acetyltransferase substrate. As opposed to findings in a previous study using the *E. coli* orthologue, galactose-derived amino sugar compounds are not substrates for *M. tuberculosis* GlmU, suggesting a stronger preference for the glucose epimer in this enzyme than in the *E. coli* homologue. UDP-GlcN was identified as a poor GlmU acetyltransferase substrate ($k_{cat}/K_{m,UDP-GlcN}$ = 2.2 × 10^2 M^{-1} s^{-1} vs $k_{cat}/K_{m,GlcN-1P}$ = 9.7 × 10^4 M^{-1} s^{-1}), while both glucosamine and GlcN-6P were not substrates for *M. tuberculosis* GlmU. The identification of UDP-GlcN as an acetyltransferase substrate, which has previously been observed for *E. coli* GlmU, raises the possibility of an alternative order of GlmU-catalyzed reactions (see Scheme 3).[28] However, it was not possible to confirm that GlcN-1P could be utilized as a substrate for uridylyl transfer by the *M. tuberculosis* GlmU. GlmU-catalyzed formation of UDP-GlcNAc from UDP-GlcN may occur in *M. tuberculosis* at a slow rate but is unlikely to constitute a physiologically important route. Therefore, the canonical order of GlmU reactions in *M. tuberculosis* is preferred.

The kinetic mechanism of GlmU acetyltransferase activity has been poorly characterized. For example, product inhibition by CoA-SH has not been described to date (Figure S6). Inhibition of *M. tuberculosis* GlmU was observed for the following Ac-CoA analogues: Bu-CoA, IsoBu-CoA, Mlo-CoA, and Cro-CoA. Inhibition by these Ac-CoA analogues is likely because of the increase in acyl thioester chain length, which will extend from the Ac-CoA binding site, protruding into the GlcN-1P site, precluding binding of GlcN-1P to GlmU. Of note, no inhibition was observed with dethio-CoA, suggesting that additional interactions with the sulfur of the *β*-

mercaptoethylamine portion of CoA-SH, reported by Jagtap et al., are required for binding.[32]

Inhibition of GlmU by GlcN-1P analogues was observed only with Glc-1P and GlcN-6P, which confirms the binding specificity for the glucose-derived epimers. Inhibition was not observed with either GlcNAc-1P or GlcNAc, which demonstrates that acetylated products have very low affinity for the substrate site. Glc-1P binding was further investigated by X-ray crystallography studies. Surprisingly, the amine from GlcN-1P and the hydroxyl of Glc-1P both occupy the exact same position in the structure, as well as the rest of the molecules. The hydroxyl in position C2 of Glc-1P is within hydrogen bonding distance of His374, suggesting that this residue could serve as the general base that deprotonates the amine prior to nucleophilic attack on Ac-CoA. A similar approach to study the Michaelis complex of *Aspergillus fumigatus* GlcN-6P *N*-acetyltransferase has been employed using Glc-6P as a pseudosubstrate in place of GlcN-6P, which helped infer the likely catalytic mechanism.[57]

DSF binding studies allowed determination of the equilibrium constant for the dissociation of Ac-CoA, Bu-CoA, CoA-SH, GlcN-1P, and Glc-1P from GlmU. Ac-CoA, Bu-CoA, and CoA-SH were able to stabilize GlmU, increasing the observed T_m by ≤4 °C, and subsequent use of the change in T_m (ΔT_m), as a function of substrate ligand concentration, allowed dissociation constants to be determined. These K_d values were broadly in agreement with the K_m and IC$_{50}$ values that were determined for these substrates, products, and dead-end inhibitors. Dissociation constants for dissociation of GlcN-1P and Glc-1P from GlmU could not be determined without Ac-CoA or an analogue present; however, in the presence of high concentrations of the second substrate, the K_d for the complex could be determined. These findings support an ordered bi-bi mechanism, where Ac-CoA or an analogue binds first followed by GlcN-1P.

The initial velocity patterns obtained are intersecting, which indicates that GlmU acetyltransferase requires the formation of a ternary complex prior to catalysis. This result rules out ping-pong mechanisms that would typically lead to the formation of an acetyl−enzyme intermediate. The patterns obtained using product and dead-end inhibitors are most consistent with a sequential ordered bi-bi kinetic mechanism (Scheme 3). Ordered binding of substrates is supported by CoA-SH acting as a competitive inhibitor versus Ac-CoA and as a non-competitive inhibitor versus GlcN-1P; the other product of the reaction, GlcNAc-1P, causes no inhibition versus either substrate. There is formation of a dead-end complex with Glc-1P, as suggested by the uncompetitive inhibition pattern versus Ac-CoA. Glc-1P inhibition versus Ac-CoA remains uncompetitive over a range of concentrations of GlcN-1P (Figure S6).

Scheme 4. Proposed GlmU Acetylation Chemical Mechanism
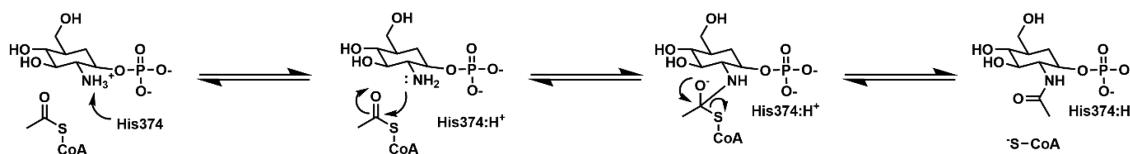
The two competitive inhibition patterns observed (Table 3) with Glc-1P versus GlcN-1P and Bu-CoA versus Ac-CoA are also characteristic of an ordered mechanism with the formation of nonproductive GlmU:Ac-CoA:Glc-1P and GlmU:Bu-CoA complexes. Bu-CoA likely extends part of its acyl chain into the GlcN-1P active site, which blocks GlcN-1P from binding, therefore appearing as competitive inhibition. Indeed, this observation is confirmed by mutual exclusivity studies performed using Bu-CoA and Glc-1P. Analysis of this experiment using the Yonetani−Theorell method confirms that these inhibitors are partially mutually exclusive. An α value of 3 was obtained from this experiment, suggesting some degree of antagonistic binding, which further confirms competition likely because of the extended acyl-thioester chain length of Bu-CoA (Figure S4).

No inhibition was observed with GlcNAc-1P versus either Ac-CoA (in the presence of varying fixed concentrations of GlcN-1P) or GlcN-1P. Although these observations would be consistent with an equilibrium ordered bi-bi kinetic mechanism, the CoA-SH inhibition pattern versus GlcN-1P is noncompetitive, which is inconsistent with the expected competitive pattern for an equilibrium ordered mechanism. A conformational change in GlmU taking place after Ac-CoA binding but before GlcN-1P binding would explain the kinetic patterns obtained (see below) and indicates that only a steady-state ordered kinetic mechanism explains the data.

The structure of GlmU with Ac-CoA and Glc-1P bound provides useful insights into formation of the catalytic as well as the dead-end inhibited ternary complexes. Inhibition by CoA-SH and Bu-CoA versus Ac-CoA, which in both cases is competitive, can be explained by the conserved recognition and binding of both the adenine ring and pantetheinyl arm of CoA, in combination with the limited interactions with the thioester bound to the β-mercaptoethylamine. It is apparent from the GlmU:Ac-CoA:Glc-1P structure that the binding sites are non-overlapping, so for any competitive inhibition to occur between dead-end analogues of the two substrates, there must be an increase in size of one or both molecules to cause either a direct steric clash or competition for binding. Superposition of the GlmU:Ac-CoA:Glc-1P structure with previously determined *M. tuberculosis* GlmU:Ac-CoA and apo structures clearly highlights that a disordered loop becomes ordered upon binding of either CoA-SH or CoA thioesters. This conformational change is likely to be facilitated through the interaction of the backbone carbonyl of Tyr398, which is located on the mobile loop, and N4P of Ac-CoA (Figure S9). The conformational change and subsequent stabilization of the mobile loop, succeeding initial Ac-CoA binding, positions Asn397 and Lys403, in addition to Tyr398, in favorable orientations to interact with either Glc-1P or GlcN-1P. These structural observations in combination with kinetic and binding data are consistent with a steady-state ordered mechanism, depicted in Scheme 2. The E:Glc-1P:Ac-CoA complex was not observed in solution, during inhibition experiments.

The ionization of the groups that may be responsible for the binding and catalysis in the GlmU-catalyzed acetyl transfer reaction was investigated by examining the pH dependence of k_{cat}, $k_{cat}/K_{m,Ac\text{-}CoA}$, and $k_{cat}/K_{m,GlcN\text{-}1P}$. The k_{cat}−pH profile revealed the presence of four nonresolvable ionizable groups, two with pK_a values of 6.7 ± 0.1 and two with pK_a values of 9.0 ± 0.1. This highlights that at least four ionizable groups contribute to steps that govern the observed rates, under V_{max} conditions. We tentatively assign His374 as the general base (pK_a of 6.7) required for deprotonation of the -NH$_3^+$ group from GlcN-1P. The other groups observed in the pH profiles cannot be easily assigned. Importantly, the two general bases (pK_a of 6.7) observed in the k_{cat}−pH profile are also present in the $k_{cat}/K_{m,Ac\text{-}CoA}$−pH profile, suggesting that these groups are also important for $k_{cat}/K_{m,Ac\text{-}CoA}$ conditions. In contrast, one ionizable group with a pK_a of 8.1 appears to be essential under $k_{cat}/K_{m,Ac\text{-}CoA}$ conditions only. The group with a pK_a of 8.1 could correspond to Tyr398, which has been shown to interact through its backbone oxygen with the oxygen atom of the acetyl, which has previously been observed with serotonin N-acetyltranferase.[58] Two general acid groups (pK_a of 9.0) were also observed in the $k_{cat}/K_{m,GlcN\text{-}1P}$−pH profile, indicating that they are also important under $k_{cat}/K_{m,GlcN\text{-}1P}$ conditions. Two general base groups (pK_a of 7.5) were also observed in the $k_{cat}/K_{m,GlcN1\text{-}P}$−pH profile, but not in the k_{cat}−pH profile. Assignment of all these ionizable groups is beyond the scope of this study. It is however noteworthy that an ionization corresponding to the amino group of GlcN-1P (pK_a of 8.4) was not observed in the k_{cat}− or $k_{cat}/K_{m,GlcN\text{-}1P}$−pH profiles. This is likely an indication that GlcN-1P binding and its deprotonation by His374 are likely not rate-limiting for acetyl transfer.

To further probe the role of H374 in catalysis, we constructed and purified the GlmU H374A mutant. This mutant was analyzed in pH−rate studies using GlcN-1P as the substrate (Figure 5). A single ionizable group that needs to be deprotonated under k_{cat} conditions was observed, which was determined to have a pK_a of 8.2 matching well the experimentally determined pK_a value for the amino group of GlcN-1P. This result indicates that deletion of the imidazolium group of H374 leads to a significant decrease in the catalytic rate (1000-fold) and a change in the rate-limiting step. In this mutant, deprotonation of GlcN-1P and therefore chemistry appears to be rate-limiting, as all other ionizable groups are no longer observed. The $k_{cat}/K_{m,\,GlcN\text{-}1P}$−pH profile suggests that a single ionizable group (pK_a of 9.7) must be deprotonated for maximal activity. This is likely an enzymic group involved in the binding of the phosphate of GlcN-1P, possibly Y377 or R344. Together, these results support the role of H374 as the general base involved in deprotonation of the amino group from GlcN-1P prior to acetyl transfer.

To assess the contribution of solvent-derived protons to the rate-limiting steps of the acetyl transfer catalyzed by GlmU, we employed SKIEs. Prior to proceeding with SKIE experiments, it is important to ensure that the effects observed are not due to the higher viscosity of D$_2$O compared to that of H$_2$O. In the

case of GlmU, the addition of 9% glycerol had small effects on only $V/K_{GlcN-1P}$. Modest but highly reproducible SKIEs of 1.57 and 1.61 on both $V_{GlcN-1P}$ and V_{Ac-CoA}, respectively, were observed, while a small SKIE of 1.34 on V/K_{Ac-CoA} was determined. These results indicate that solvent-sensitive steps (such as the deprotonation of GlcN-1P) are partially rate-limiting for acetyl transfer. The similar magnitude of the SKIEs on both substrates indicates that deprotonation of GlcN-1P might be partially rate-limiting; however, this group was not observed on the pH profile. Together, these small SKIEs indicate that steps other than chemistry are likely rate-limiting for GlmU-catalyzed acetyl transfer.

Chemical Mechanism. The results presented here define three important facets of the chemical mechanism used by GlmU to acetylate GlcN-1P (Scheme 4). First, the intersecting initial velocity patterns and the product inhibition studies rule out ping-pong mechanisms and confirm that GlmU acetylates GlcN-1P by a direct mechanism. Second, the α-amino of GlcN-1P is in its protonated form when it binds to GlmU, and therefore, the first essential step in catalysis is the deprotonation of this α-amino group by a general base. The side chain imidazole of His374 both is optimally positioned and has the right pK_a to be able to abstract this proton. In addition, the active site histidine residues have been observed in other acetyltransferases that use a ternary complex mechanism, such as GlmU.[59] Third, chemistry is likely to be partially rate-limiting as both pH−rate studies and solvent kinetic isotope effects indicate the presence of critical groups involved in catalysis and substrate binding as well as solvent-mediated proton transfers that are partially rate-limiting for the acetyl transfer reaction.

CONCLUSIONS

M. tuberculosis *N*-acetyltransferase, uridylyltransferase GlmU requires Mg^{2+} for optimal acetyltransferase activity and follows a steady-state ordered sequential mechanism, with Ac-CoA as the first substrate to bind. Binding of Ac-CoA triggers a conformational change that allows GlcN-1P to bind. After chemistry, GlcNAc-1P dissociates followed by CoA-SH. An active site conformational change (loop closure) occurs upon CoA-SH or acyl-CoA binding (consistent with previously studied LβH acetyltransferases). pH−rate studies support the existence of a general base-catalyzed step in the reaction mechanism, proposed to be $N^{\epsilon 2}$ of the imidazole side chain of His374, which abstracts a proton from the NH_3^+ group of GlcN-1P, to prime the α-amino group for nucleophilic attack on the acetyl group of Ac-CoA. Although His374 is proposed to be the general base, deprotonation of GlcN-1P was not identified as the rate-limiting step for GlmU-catalyzed acetyl transfer. Solvent kinetic isotope effect studies identified that a chemical step involving a solvent-derived proton is critical for GlmU acetyltransferase activity. The mechanistic features of GlmU acetyltransferase activity revealed by these studies are invaluable for the future rational design of novel GlmU inhibitors that may be used in the treatment of tuberculosis.

ASSOCIATED CONTENT

Ⓢ Supporting Information

The Supporting Information is available free of charge on the ACS Publications website at DOI: 10.1021/acs.biochem.8b00121.

Supplementary methods, tables, figures, and data (PDF)

AUTHOR INFORMATION

Corresponding Authors
*E-mail: luiz.carvalho@crick.ac.uk.
*E-mail: argyrides.argyrou@astrazeneca.com.

ORCID 🄳
Robert J. Young: 0000-0002-7763-0575
Luiz Pedro S. de Carvalho: 0000-0003-2875-4552

Present Address
⊥A.A.: Discovery Biology, Discovery Sciences, IMED Biotech unit, AstraZeneca, Cambridge, U.K.

REFERENCES

(1) Global Tuberculosis Report 2017 (2017) World Health Organization, Geneva.
(2) Gygli, S. M., Borrell, S., Trauner, A., and Gagneux, S. (2017) Antimicrobial resistance in Mycobacterium tuberculosis: mechanistic and evolutionary perspectives. *FEMS Microbiology Reviews 41*, 354−373.
(3) Jackson, M. (2014) The Mycobacterial Cell Envelope—Lipids. *Cold Spring Harbor Perspect. Med. 4*, a021105.
(4) Jankute, M., Cox, J. A. G., Harrison, J., and Besra, G. S. (2015) Assembly of the Mycobacterial Cell Wall. *Annu. Rev. Microbiol. 69*, 405−423.
(5) Daffé, M. (2015) The cell envelope of tubercle bacilli. *Tuberculosis 95*, S155−S158.
(6) Bugg, T. D. H., Braddick, D., Dowson, C. G., and Roper, D. I. (2011) Bacterial cell wall assembly: still an attractive antibacterial target. *Trends Biotechnol. 29*, 167−173.
(7) Abrahams, K. A., and Besra, G. S. (2018) Mycobacterial cell wall biosynthesis: a multifaceted antibiotic target. *Parasitology 145*, 116−133.
(8) Mendes, V., and Blundell, T. L. (2017) Targeting tuberculosis using structure-guided fragment-based drug design. *Drug Discovery Today 22*, 546−554.
(9) Bugg, T. D. H., and Walsh, C. T. (1992) Intracellular steps of bacterial cell wall peptidoglycan biosynthesis: enzymology, antibiotics, and antibiotic resistance. *Nat. Prod. Rep. 9*, 199−215.

(10) Durand, P., Golinelli-Pimpaneau, B., Mouilleron, S., Badet, B., and Badet-Denisot, M.-A. (2008) Highlights of glucosamine-6P synthase catalysis. *Arch. Biochem. Biophys. 474*, 302−317.

(11) Mengin-Lecreulx, D., and van Heijenoort, J. (1996) Characterization of the Essential Gene glmM Encoding Phosphoglucosamine Mutase in Escherichia coli. *J. Biol. Chem. 271*, 32−39.

(12) Mengin-Lecreulx, D., and van Heijenoort, J. (1993) Identification of the glmU gene encoding N-acetylglucosamine-1-phosphate uridyltransferase in Escherichia coli. *J. Bacteriol. 175*, 6150−6157.

(13) Mengin-Lecreulx, D., and van Heijenoort, J. (1994) Copurification of glucosamine-1-phosphate acetyltransferase and N-acetylglucosamine-1-phosphate uridyltransferase activities of Escherichia coli: characterization of the glmU gene product as a bifunctional enzyme catalyzing two subsequent steps in the pathway for UDP-N-acetylglucosamine synthesis. *J. Bacteriol. 176*, 5788−5795.

(14) Olsen, L. R., and Roderick, S. L. (2001) Structure of the Escherichia coli GlmU Pyrophosphorylase and Acetyltransferase Active Sites. *Biochemistry 40*, 1913−1921.

(15) Sulzenbacher, G., Gal, L., Peneff, C., Fassy, F., and Bourne, Y. (2001) Crystal Structure of Streptococcus pneumoniae N-Acetylglucosamine-1-phosphate Uridyltransferase Bound to Acetyl-coenzyme A Reveals a Novel Active Site Architecture. *J. Biol. Chem. 276*, 11844−11851.

(16) Mochalkin, I., Lightle, S., Narasimhan, L., Bornemeier, D., Melnick, M., VanderRoest, S., and McDowell, L. (2008) Structure of a small-molecule inhibitor complexed with GlmU from Haemophilus influenzae reveals an allosteric binding site. *Protein Sci. 17*, 577−582.

(17) Zhang, Z., Bulloch, E. M. M., Bunker, R. D., Baker, E. N., and Squire, C. J. (2009) Structure and function of GlmU from Mycobacterium tuberculosis. *Acta Crystallogr., Sect. D: Biol. Crystallogr. 65*, 275−283.

(18) Pye, V. E., Tingey, A. P., Robson, R. L., and Moody, P. C. E. (2004) The Structure and Mechanism of Serine Acetyltransferase from Escherichia coli. *J. Biol. Chem. 279*, 40729−40736.

(19) Wang, X.-G., Olsen, L. R., and Roderick, S. L. (2002) Structure of the lac Operon Galactoside Acetyltransferase. *Structure 10*, 581−588.

(20) Lo Leggio, L., Dal Degan, F., Poulsen, P., Andersen, S. M., and Larsen, S. (2003) The Structure and Specificity of Escherichia coli Maltose Acetyltransferase Give New Insight into the LacA Family of Acyltransferases. *Biochemistry 42*, 5225−5235.

(21) Robins, L. I., Williams, A. H., and Raetz, C. R. H. (2009) Structural Basis for the Sugar Nucleotide and Acyl-Chain Selectivity of Leptospira interrogans LpxA. *Biochemistry 48*, 6191−6201.

(22) Bartling, C. M., and Raetz, C. R. H. (2008) Steady-State Kinetics and Mechanism of LpxD, the N-Acyltransferase of Lipid A Biosynthesis. *Biochemistry 47*, 5290−5302.

(23) Vetting, M. W., S. de Carvalho, L. P., Yu, M., Hegde, S. S., Magnet, S., Roderick, S. L., and Blanchard, J. S. (2005) Structure and functions of the GNAT superfamily of acetyltransferases. *Arch. Biochem. Biophys. 433*, 212−226.

(24) Pompeo, F., Bourne, Y., van Heijenoort, J., Fassy, F., and Mengin-Lecreulx, D. (2001) Dissection of the Bifunctional Escherichia coli N-Acetylglucosamine-1-phosphate Uridyltransferase Enzyme into Autonomously Functional Domains and Evidence That Trimerization Is Absolutely Required for Glucosamine-1-phosphate Acetyltransferase Activity and Cell Growth. *J. Biol. Chem. 276*, 3833−3839.

(25) Wang, J., Liu, X., Liang, Y.-H., Li, L.-F., and Su, X.-D. (2008) Acceptor substrate binding revealed by crystal structure of human glucosamine-6-phosphate N-acetyltransferase 1. *FEBS Lett. 582*, 2973−2978.

(26) Mio, T., Yamada-Okabe, T., Arisawa, M., and Yamada-Okabe, H. (2000) Functional cloning and mutational analysis of the human cDNA for phosphoacetylglucosamine mutase: identification of the amino acid residues essential for the catalysis11The GenBank/EMBL/DDBJ accession numbers for the nucleotide sequences of HsAGM1, and CaAGM1 are AB032081 and AB032082, respectively. *Biochim. Biophys. Acta, Gene Struct. Expression 1492*, 369−376.

(27) Peneff, C., Ferrari, P., Charrier, V., Taburet, Y., Monnier, C., Zamboni, V., Winter, J., Harnois, M., Fassy, F., and Bourne, Y. (2001) Crystal structures of two human pyrophosphorylase isoforms in complexes with UDPGlc(Gal)NAc: role of the alternatively spliced insert in the enzyme oligomeric assembly and active site architecture. *EMBO J. 20*, 6191−6202.

(28) Gehring, A. M., Lees, W. J., Mindiola, D. J., Walsh, C. T., and Brown, E. D. (1996) Acetyltransfer Precedes Uridylyltransfer in the Formation of UDP-N-acetylglucosamine in Separable Active Sites of the Bifunctional GlmU Protein of Escherichia coli. *Biochemistry 35*, 579−585.

(29) Sassetti, C. M., Boyd, D. H., and Rubin, E. J. (2003) Genes required for mycobacterial growth defined by high density muta-genesis. *Mol. Microbiol. 48*, 77−84.

(30) Zhang, W., Jones, V. C., Scherman, M. S., Mahapatra, S., Crick, D., Bhamidi, S., Xin, Y., McNeil, M. R., and Ma, Y. (2008) Expression, essentiality, and a microtiter plate assay for mycobacterial GlmU, the bifunctional glucosamine-1-phosphate acetyltransferase and N-acetyl-glucosamine-1-phosphate uridyltransferase. *Int. J. Biochem. Cell Biol. 40*, 2560−2571.

(31) Soni, V., Upadhayay, S., Suryadevara, P., Samla, G., Singh, A., Yogeeswari, P., Sriram, D., and Nandicoori, V. K. (2015) Depletion of M. tuberculosis GlmU from Infected Murine Lungs Effects the Clearance of the Pathogen. *PLoS Pathog. 11*, e1005235.

(32) Jagtap, P. K. A., Soni, V., Vithani, N., Jhingan, G. D., Bais, V. S., Nandicoori, V. K., and Prakash, B. (2012) Substrate-bound Crystal Structures Reveal Features Unique to Mycobacterium tuberculosis N-Acetyl-glucosamine 1-Phosphate Uridyltransferase and a Catalytic Mechanism for Acetyl Transfer. *J. Biol. Chem. 287*, 39524−39537.

(33) Morais, L. L., Yuasa, H., Bennis, K., Ripoche, I., and Auzanneau, F.-I. (2006) Chemoenzymatic synthesis of thio-nod factor intermediates — Enzymatic transfer of glucosamine on thiochitobiose derivatives. *Can. J. Chem. 84*, 587−596.

(34) Vazquez, M. J., Rodriguez, B., Zapatero, C., and Tew, D. G. (2003) Determination of phosphate in nanomolar range by an enzyme-coupling fluorescent method. *Anal. Biochem. 320*, 292−298.

(35) Brune, M., Hunter, J. L., Corrie, J. E. T., and Webb, M. R. (1994) Direct, Real-Time Measurement of Rapid Inorganic Phosphate Release Using a Novel Fluorescent Probe and Its Application to Actomyosin Subfragment 1 ATPase. *Biochemistry 33*, 8262−8271.

(36) Beckonert, O., Keun, H. C., Ebbels, T. M. D., Bundy, J., Holmes, E., Lindon, J. C., and Nicholson, J. K. (2007) Metabolic profiling, metabolomic and metabonomic procedures for NMR spectroscopy of urine, plasma, serum and tissue extracts. *Nat. Protoc. 2*, 2692.

(37) Kay, L., Keifer, P., and Saarinen, T. (1992) Pure absorption gradient enhanced heteronuclear single quantum correlation spectroscopy with improved sensitivity. *J. Am. Chem. Soc. 114*, 10663−10665.

(38) Baryshnikova, O. K., Williams, T. C., and Sykes, B. D. (2008) Internal pH indicators for biomolecular NMR. *J. Biomol. NMR 41*, 5−7.

(39) Oregioni, A., Stieglitz, B., Kelly, G., Rittinger, K., and Frenkiel, T. (2017) Determination of the pKa of the N-terminal amino group of ubiquitin by NMR. *Sci. Rep. 7*, 43748.

(40) Derome, A. E., and Williamson, M. P. (1990) Rapid-pulsing artifacts in double-quantum-filtered COSY. *J. Magn. Reson. (1969-1992) 88*, 177−185.

(41) Ellis, K. J., and Morrison, J. F. (1982) [23] Buffers of constant ionic strength for studying pH-dependent processes. In *Methods in Enzymology* (Purich, D. L., Ed.) pp 405−426, Academic Press.

(42) Northrop, D. B. (1981) The Expression of Isotope Effects on Enzyme-Catalyzed Reactions. *Annu. Rev. Biochem. 50*, 103−131.

(43) Winter, G., Lobley, C. M. C., and Prince, S. M. (2013) Decision making in xia2. *Acta Crystallogr., Sect. D: Biol. Crystallogr. 69*, 1260−1273.

(44) Jagtap, P. K. A., Verma, S. K., Vithani, N., Bais, V. S., and Prakash, B. (2013) Crystal Structures Identify an Atypical Two-Metal-Ion Mechanism for Uridyltransfer in GlmU: Its Significance to Sugar Nucleotidyl Transferases. *J. Mol. Biol. 425*, 1745−1759.

(45) McCoy, A. J., Grosse-Kunstleve, R. W., Adams, P. D., Winn, M. D., Storoni, L. C., and Read, R. J. (2007) Phaser crystallographic software. *J. Appl. Crystallogr. 40*, 658−674.

(46) Adams, P. D., Afonine, P. V., Bunkoczi, G., Chen, V. B., Davis, I. W., Echols, N., Headd, J. J., Hung, L.-W., Kapral, G. J., Grosse-Kunstleve, R. W., McCoy, A. J., Moriarty, N. W., Oeffner, R., Read, R. J., Richardson, D. C., Richardson, J. S., Terwilliger, T. C., and Zwart, P. H. (2010) PHENIX: a comprehensive Python-based system for macromolecular structure solution. *Acta Crystallogr., Sect. D: Biol. Crystallogr. 66*, 213−221.

(47) Emsley, P., Lohkamp, B., Scott, W. G., and Cowtan, K. (2010) Features and development of Coot. *Acta Crystallogr., Sect. D: Biol. Crystallogr. 66*, 486−501.

(48) Vaguine, A. A., Richelle, J., and Wodak, S. J. (1999) SFCHECK: a unified set of procedures for evaluating the quality of macromolecular structure-factor data and their agreement with the atomic model. *Acta Crystallogr., Sect. D: Biol. Crystallogr. 55*, 191−205.

(49) *The PyMOL Molecular Graphics System*, version 1.3r1 (2010) Schrödinger, LLC.

(50) Skoog, D. A., and West, D. M. (1982) *Fundamentals of Analytical Chemistry*, Saunders College Publishing, Philadelphia.

(51) Olsen, L. R., Vetting, M. W., and Roderick, S. L. (2007) Structure of the E. coli bifunctional GlmU acetyltransferase active site with substrates and products. *Protein Sci. 16*, 1230−1235.

(52) Lewendon, A., Murray, I. A., Kleanthous, C., Cullis, P. M., and Shaw, W. V. (1988) Substitutions in the active site of chloramphenicol acetyltransferase: role of a conserved aspartate. *Biochemistry 27*, 7385−7390.

(53) Schuldt, L., Weyand, S., Kefala, G., and Weiss, M. S. (2009) The Three-dimensional Structure of a Mycobacterial DapD Provides Insights into DapD Diversity and Reveals Unexpected Particulars about the Enzymatic Mechanism. *J. Mol. Biol. 389*, 863−879.

(54) Pompeo, F., van Heijenoort, J., and Mengin-Lecreulx, D. (1998) Probing the Role of Cysteine Residues in Glucosamine-1-Phosphate Acetyltransferase Activity of the Bifunctional GlmU Protein fromEscherichia coli: Site-Directed Mutagenesis and Characterization of the Mutant Enzymes. *J. Bacteriol. 180*, 4799−4803.

(55) Buurman, E. T., Andrews, B., Gao, N., Hu, J., Keating, T. A., Lahiri, S., Otterbein, L. R., Patten, A. D., Stokes, S. S., and Shapiro, A. B. (2011) In Vitro Validation of Acetyltransferase Activity of GlmU as an Antibacterial Target in Haemophilus influenzae. *J. Biol. Chem. 286*, 40734−40742.

(56) Zhou, Y., Xin, Y., Sha, S., and Ma, Y. (2011) Kinetic properties of Mycobacterium tuberculosis bifunctional GlmU. *Arch. Microbiol. 193*, 751.

(57) Hurtado-Guerrero, R., Raimi, O., Shepherd, S., and van Aalten, D. M. F. (2007) Glucose-6-phosphate as a probe for the glucosamine-6-phosphate N-acetyltransferase Michaelis complex. *FEBS Lett. 581*, 5597−5600.

(58) Scheibner, K. A., De Angelis, J., Burley, S. K., and Cole, P. A. (2002) Investigation of the Roles of Catalytic Residues in SerotoninN-Acetyltransferase. *J. Biol. Chem. 277*, 18118−18126.

(59) Johnson, C. M., Roderick, S. L., and Cook, P. F. (2005) The serine acetyltransferase reaction: acetyl transfer from an acylpantothenyl donor to an alcohol. *Arch. Biochem. Biophys. 433*, 85−95.